ELSEVIER

Journal of Electroanalytical Chemistry 381 (1995) 99–104

JOURNAL OF ELECTROANALYTICAL CHEMISTRY

Ohmic distortion of current–potential curves at wall-jet electrodes

Barry A. Coles [*,a], Richard G. Compton [a], Christopher M.A. Brett [b], Ana Maria C.F. Oliveira Brett [b]

[a] *Physical Chemistry Laboratory, Oxford University, South Parks Road, Oxford OX1 3QZ, UK*
[b] *Departamento de Química, Universidade de Coimbra, P-3049 Coimbra, Portugal*

Received 10 June 1994; in revised form 1 August 1994

Abstract

The ohmic distortion of current–voltage curves for the wall-jet hydrodynamic electrode is investigated using a finite-element approach with the circuit analysis program SPICE. Simulated and experimental data are presented, showing the displacement of the half-wave potential and the potential-dependent error in the Tafel slope. Error curves are given as a guide to the maximum current levels which may be used in practice with different electrolyte concentrations.

Keywords: Ohmic distortion; Current–potential curves

1. Introduction

The wall-jet electrode [1], in which a fine, submerged jet of fluid hits the centre of a disc electrode and spreads out radially, is useful for in-line flow analysis systems [2]; its hydrodynamic characteristics provide very non-uniform access to the electrode for reacting species, which can be advantageous in elucidating electrode reaction mechanisms [3]. For both applications it is important that the measured data are not subject to systematic errors. However, the solution resistance may cause the potential and the primary current distribution over the electrode to be distorted, and a further factor with the wall-jet arrangement is that for hydrodynamic reasons the reference electrode cannot readily be positioned close to the working electrode, so the uncompensated cell resistance is usually high. These effects can cause errors in the observed values for the half-wave potential and the Tafel slope, which under normal operating conditions may be significant even when high concentrations of background electrolyte are used. The purpose of this paper is to evaluate the magnitude of these errors and establish conditions under which they may be neglected.

Analytical treatment of resistive distortion has been restricted to cells of simple geometry; for more complex geometries, numerical methods employing finite-element techniques have proved advantageous [4]. In this work a finite-element approach based on a resistor network representation of the solution, first applied to channel electrodes [5], has been used to estimate these effects as a function of the limiting current, and the predictions have been confirmed using experimental data. Curves are presented which may be used to estimate the errors under given experimental conditions, as a guide to practical working limits.

2. Experimental details

The wall-jet cell used (Fig. 1) was as described in previous work [6] and is of large volume to allow unrestricted flow hydrodynamics, with a diameter of 80 mm. The platinum electrode radius was 1.637 mm and the inlet nozzle was of internal diameter 0.345 mm. The nozzle–electrode distance was fixed at 2 mm. The SCE reference electrode could be placed either downstream within the cell in a region of low potential gradients, or upstream within the flow system before the jet. As the downstream position of the reference electrode departs from axial symmetry, the potential distribution in the cell and hence the effective uncompensated resistance R_u was determined from a three-dimensional analysis using the ANSYS general-purpose finite-element program (version 5.0, Swanson Analysis

* Corresponding author.

SSDI 0022-0728(94)03692-6

Systems Inc., Houston, USA). One half of the cell was modelled using a mesh of 6130 thermal-electric SOLID69 elements, with resistivity set equal to that of the electrolyte. Nodes corresponding to the working electrode position were set to zero voltage, and those corresponding to the counter-electrode were set to 1 V. The potential distribution was then calculated, and selected values are shown as contours in Fig. 1. The downstream reference electrode position is at a potential of 0.755 V, corresponding to an effective uncompensated resistance value of 0.755 of the total cell resistance. The potential at the jet position is 0.38 V, so the upstream reference electrode position would give a lower R_u of 0.38 of the cell resistance.

Experimental data were obtained from the voltammetric curves for the oxidation of 5.0 mM $K_4Fe(CN)_6$ in aqueous solution at 20°C with 0.4 M K_2SO_4 as supporting electrolyte. Flow rates up to 0.4 $cm^3\ s^{-1}$ were employed, giving limiting currents in the range 94 to 1016 μA; over this range, flow rates were adequate to ensure that the radial variation of the current density on the electrode would be proportional to $r^{-5/4}$ in the absence of resistive effects, as required for a transport-controlled process [7]. Measurements were made with a Solartron 1286 Electrochemical Interface, point by point at 5 mV intervals, with a scan rate of 3 s per step. The electrolyte conductivity was calculated from published data [8].

For studying the ohmic distortion effects, the cell with its electrodes was represented as an electrical

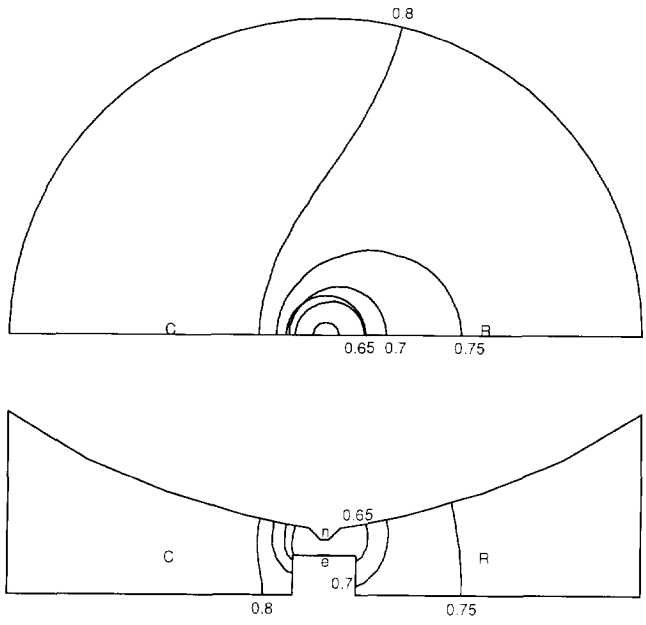

Fig. 1. Horizontal (one half shown) and vertical cross-sections of the wall-jet cell showing contours for the intervals 0.65, 0.7, 0.75 and 0.8 of total cell resistance. Horizontal contours are in the plane of the working electrode. C, R indicate the positions of the counter- and reference electrodes; n, nozzle; e, working electrode.

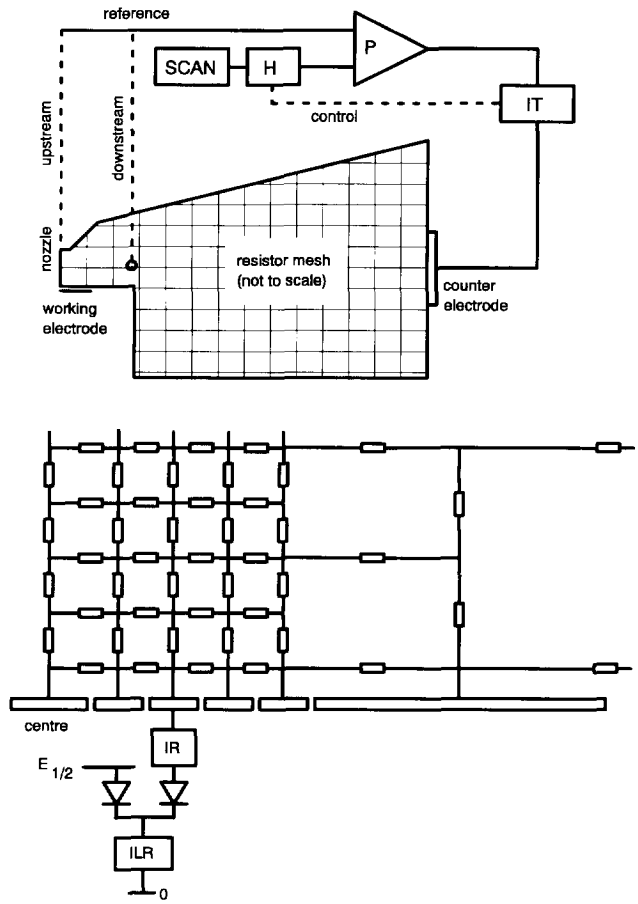

Fig. 2. Schematic circuit for the simulation, with detail of the central part of the resistor mesh. SCAN, scan generator; P, potentiostat amplifier; IT, total current measurement; H, optional voltage source controlled by the total current; IR, current measurement for one electrode ring element; ILR, current source set at the limiting current value for one electrode ring element. Only one double-diode circuit is shown for clarity.

circuit and the behaviour of the circuit was solved using the SPICE program (version 3C1, on a Sun Microsystems 670MP). SPICE is a general-purpose program for the simulation of electrical circuits, which must be defined in the form of a set of connection points (nodes) and a list of components, and with each component specification listing the nodes to which it is connected. The advantage of using SPICE is that it allows a circuit to be set up which yields analytically correct behaviour equivalent to a reversible electrode process [5].

The solution was modelled as a two-dimensional network of resistors (Fig. 2), with each resistor corresponding to an element of the solution. By considering the central rotational axis of symmetry of the cell, each resistor in the two-dimensional representation was given a value appropriate to the volume of the annular ring of solution formed by a 2π rotation of a corresponding area element about the axis. Thus radial resistors had values determined from $[\ln(r_2/r_1)]/2\pi\kappa h$,

and axial resistors from $h/\kappa\pi(r_2^2 - r_1^2)$, where r_1, r_2 denoted the inner and outer radial distance of an element, h was the axial dimension, and κ was the solution conductivity. The mesh extended from the centre of the cell for a radial distance of 20 mm. The mesh (element) size was 16.37 μm (radial) $\times$ 25 μm (axial) adjacent to the centre of the electrode, increasing to 1 mm (axial) $\times$ 4 mm (radial) in the outer parts of the cell. The counter-electrode was represented by a connection to a set of parallel resistors attached to nodes on the outer edge of the mesh. For the upstream position of the reference electrode, the connection was similarly made to nodes of the mesh inside the nozzle. The alternative downstream position of the reference electrode was made by a connection to a node within the mesh, positioned at the same fraction of total cell resistance as that determined for the reference electrode in the three-dimensional finite-element analysis. The simulation for counter- and reference electrodes was completed by the inclusion of a potentiostat circuit and scan generator [5].

In order to investigate the radial current distribution, the working electrode was treated as being divided into 20 annular elements at equal radial increments of 81.85 μm, with the innermost element, where gradients are highest, being further subdivided in steps of 16.37 μm. Over the electrode radius, the resistor mesh spacing corresponded to the electrode element spacing, and the central disc and the annular rings were represented by connections to separate nodes on the mesh (Fig. 2) of a set of 24 double-diode circuits. The limiting current for each of the electrode elements was set to the value $i_L^{ring} = I_L^{total}(x_2^{3/4} - x_1^{3/4})$, where I_L^{total} was the limiting current for the whole electrode, and x_1 and x_2 were the inner and outer fractional radii of the element, $(0 \leq x \leq 1)$, by using appropriate parameters to define the current sources (ILR in Fig. 2). SPICE was then used to carry out a static d.c. analysis at 5 mV intervals over a scan range of 0.05 to 0.55 V, with the half-wave potential set at 0.224 V.

3. Results and discussion

Fig. 3 shows the simulated radial current distribution for a limiting current of 992 μA as a function of the applied potential with the reference downstream. This indicates that while the current at the edge of the electrode reached 99% of its limiting value by $E_{1/2}$ + 128 mV, the current to the central element develops more slowly and only reached 99% of the limiting value by $E_{1/2}$ + 293 mV. Current to some of the innermost elements may be lower than the current to outer parts of the electrode over part of the potential range.

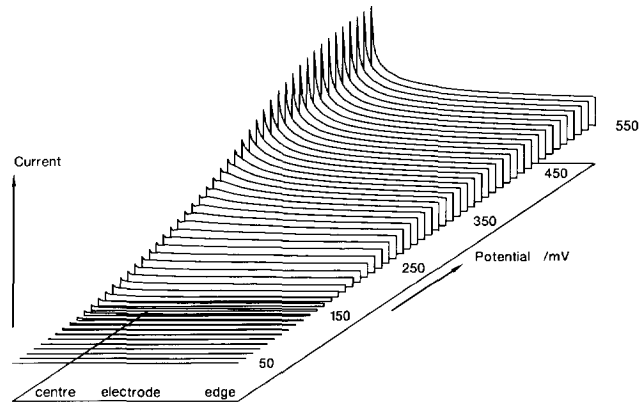

Fig. 3. Radial current distribution on the electrode as a function of the scan potential.

Fig. 4 shows the simulated values predicted for the Tafel slope for currents of 992 μA and 216 μA, together with the experimentally determined values, for the case of the reference electrode downstream. It will be seen that there is substantial departure from the expected value of −58.17 mV per decade (20°C) for reversible reactions, particularly at the higher current, and that there is good agreement between the simulation and the experiment. The results for the reference electrode upstream are similar (Fig. 5), although the experimental points exhibit greater scatter, which is attributed to the high electrical resistance of the solution channel through the nozzle allowing an increased noise level. The Tafel slope was obtained by evaluating $\delta V/\delta\{\log[(I_L/I) - 1]\}$, where V was the potential difference between the working and reference electrodes, from the differences between adjacent points. This procedure retains the shape of the variation but is very sensitive to any noise on the data.

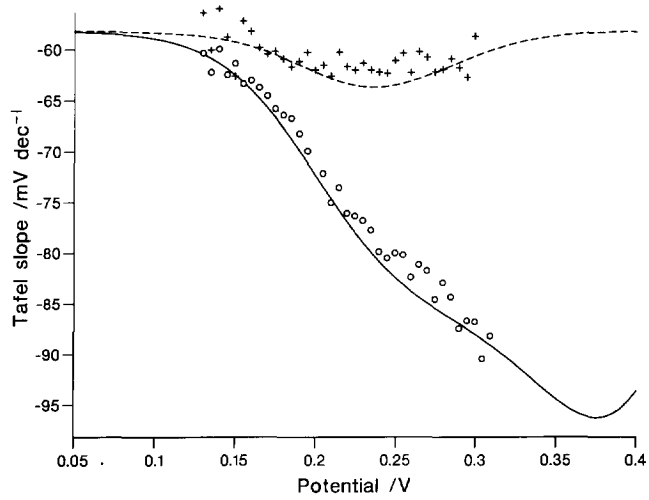

Fig. 4. Simulated curves and experimental points for the Tafel slope with the reference electrode downstream: solid line and ○, 992 μA; dashed line and +, 216 μA.

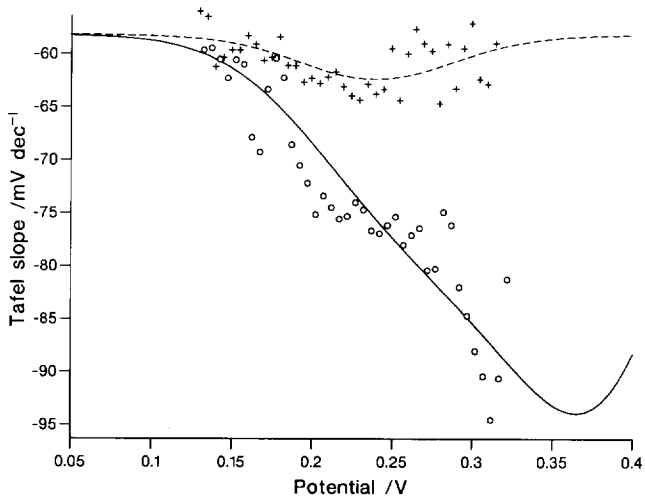

Fig. 5. Simulated curves and experimental points for the Tafel slope with the reference electrode upstream: solid line and ○: 972 μA, dashed line and +, 212.5 μA.

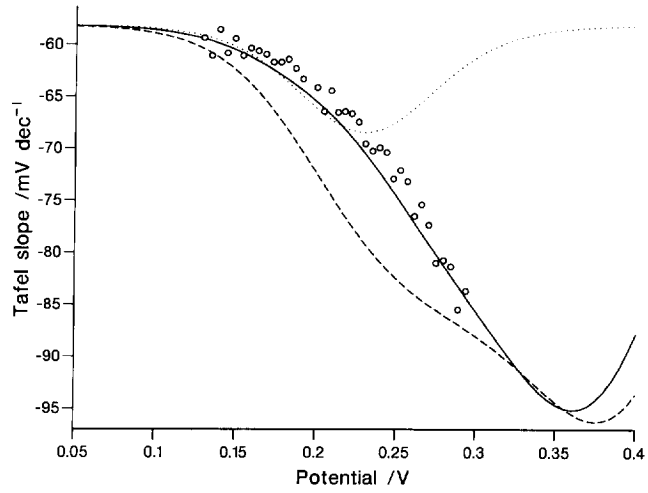

Fig. 6. Simulated curve (solid line) and experimental points for the Tafel slope with correction for the uncompensated resistance at 992 μA, without correction (dashed line), and the contribution from uncompensated resistance alone (dotted line). Reference electrode downstream.

The simulations show that the uncompensated resistance R_u, representing the bulk resistance of the solution between the working electrode and the equipotential surface on which the reference electrode lies, only contributes a small proportion of the observed errors. If this resistance is treated as a fixed single value, circuitry may be used in the potentiostat to provide an active correction for this source of error. The R_u distortion is readily calculated as part of the SPICE simulations. The effect of adding R_u compensation in the potentiostat was also simulated in the SPICE model, as shown in the schematic circuit in Fig. 2, by using the SPICE H element (a current-controlled voltage source) to displace the scan voltage by an amount equal to $R_u \times$ (total current).

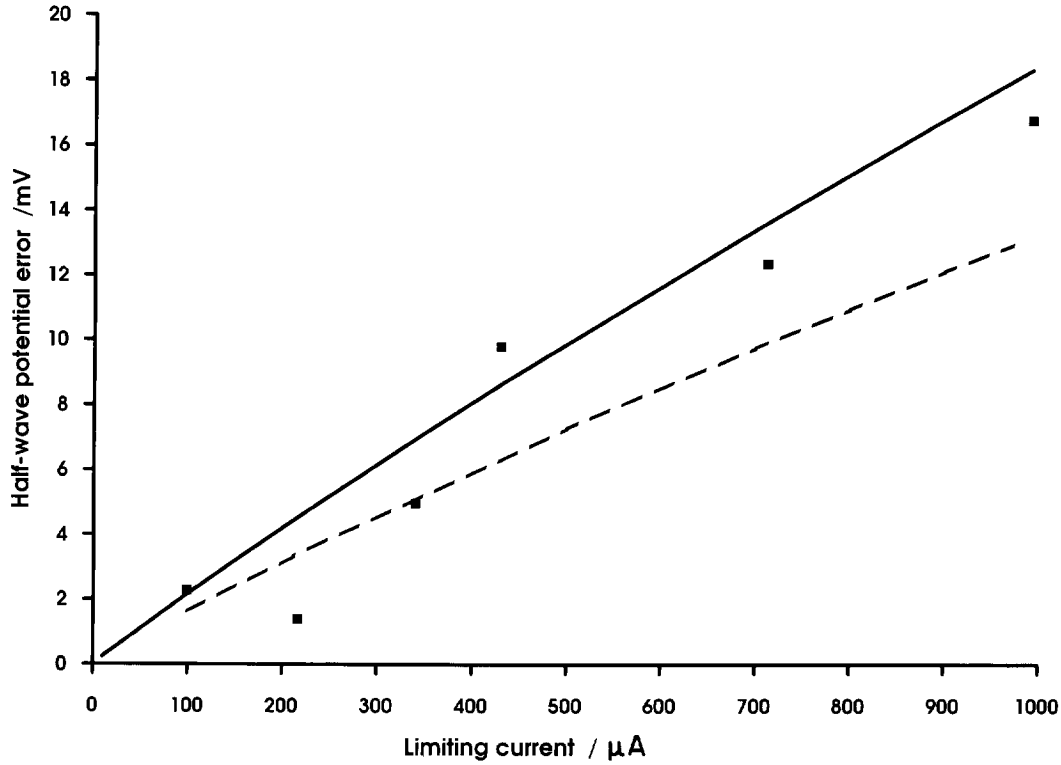

Fig. 7. Displacement of the half-wave potential calculated for the reference electrode downstream (solid line) and upstream (dashed line), with experimental points for the reference downstream, as a function of the limiting current.

The results are shown in Fig. 6 for a limiting current of 992 μA, where the full line shows the simulated Tafel slope with R_u compensation included. For comparison, the dashed line shows the uncompensated behaviour as in Fig. 4. The experimental points shown are derived from the same data as used in Fig. 4, but compensated for R_u by adjusting the potential coordinate for each data point by an amount equal to $R_u \times$ (total current). The dotted line is the result which would be expected from R_u alone, giving a maximum error in Tafel slope of -10.3 mV at a potential of $E_{1/2} + 5$ mV, returning to zero at higher potentials as I_L is approached. The effect of R_u in the wall-jet cell is to broaden the wave by displacing each point by an amount IR_u, up to a maximum of $I_L R_u$: in this example, where $R_u = 20.2\ \Omega$, the top of the wave would be displaced by 20 mV.

It is therefore clear that the major part of the error does not arise from the conventional single-valued R_u, and it cannot be removed by applying IR_u correction, either in the potentiostat or by post-processing the data as in Fig. 6. This error is caused by the distribution of potential over the working electrode surface and from the changes in that distribution. While this distribution does of course occur because of the solution resistance, it cannot usefully be treated as uncompensated resistance, since a different value of resistor would be required for each electrode element, and these resistor values would change as the current distribution, and hence the current paths, altered. Compensation for a distribution of R_u values would only be correct for one element, and, as the current distribution altered, the correctly compensated point on the electrode would move. In the present example with $I_L = 992\ \mu$A, when the input or scan potential is set to $E_{1/2} + 100$ mV, the potential difference between the centre and the edge of the working electrode is 96 mV. The edge of the electrode is at $E_{1/2} + 88$ mV, an offset slightly less than the IR_u drop (16 mV), whereas the centre is at a potential of $E_{1/2} - 8$ mV, a deviation some seven times greater than IR_u. This distortion of potential is most severe for the central region of the electrode, with half of the 96 mV difference occurring over the innermost 5% of the electrode radius.

The two-dimensional SPICE representation shows good agreement with the experimental data, which indicates that it provided a very close approximation to the (three-dimensional) cell behaviour. Whilst the position of the counter-electrode at one side of the cell departs from axial symmetry, the low resistance path provided by the large bulk of surrounding solution is clearly effective in minimizing any further contribution to distortion from this source.

Fig. 7 shows the simulated values for the displacement of the observed half-wave potential as a function of limiting current for both upstream and downstream positions of the reference electrode, together with the experimental points for the downstream position. The undistorted half-wave potential for this set of experimental data was estimated to be 0.224 mV from the curve with the lowest limiting current (99 μA), and assuming 0.002 V displacement in accordance with the

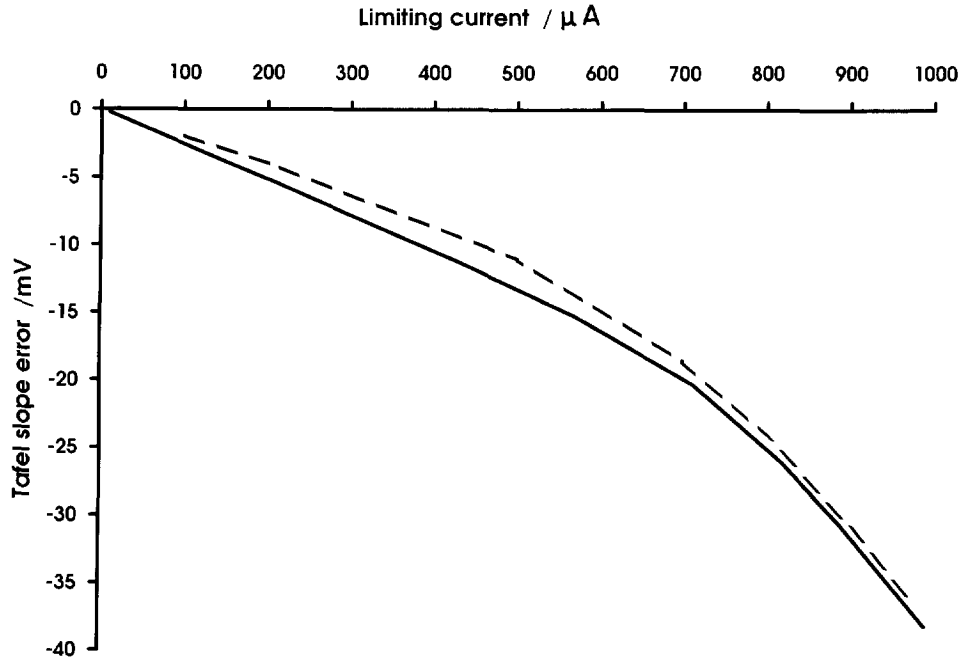

Fig. 8. Maximum error calculated for the Tafel slope as a function of the limiting current. Reference electrode downstream (solid line) and upstream (dashed line).

almost linear variation predicted by the simulation. A smaller error is expected for the upstream position, corresponding to the reduced fraction of uncompensated cell resistance. Fig. 8 shows the maximum error predicted for Tafel slope as a function of the limiting current. Both positions of the reference electrode give similar results, reflecting the relatively small contribution to Tafel slope error from uncompensated resistance.

The errors introduced by solution resistance for the wall-jet electrode as shown in Figs. 7 and 8 are quite distinct from those found for the channel electrode [5], when the latter is operated in the most usual configuration with the reference and counter-electrodes at opposite ends of the channel. The displacement of the observed half-wave potential with the wall-jet is towards higher voltages, instead of lower; the magnitude of the displacement for equivalent electrode current and solution conductivity is a factor of two greater than for the channel. The error in Tafel slope (relative to −58.17 mV per decade) is in the negative direction for the wall-jet, and for higher currents it continues to increase over and beyond the practicable experimental range. This is in marked contrast to the channel, where the error for low currents is positive, and for higher currents is positive followed by negative, but returning to a small value at higher potentials. These differences arise because the interaction between solution resistance and current has opposite consequences in the two types of cell. For the channel when current is flowing, the reference electrode indicates the potential at or very close to one end of the working electrode; higher potentials are applied to the rest of the electrode and these potentials increase with increasing current. For the wall-jet with current flowing, the potentials applied to the working electrode are everywhere lower than that indicated by the reference electrode, with the lowest potential being at the centre of the electrode, and these potentials decrease relative to the reference electrode as current is increased.

The error curves may be applied to wall-jet cells of other dimensions, provided that they meet the criteria for electrochemical "wall-jet" behaviour, i.e. that flow rates, geometry and electrode radius are such as to set up non-uniform access with current density for a transport-controlled process varying as $r^{-5/4}$. Thus, electrode radius must be large enough to avoid uniform-access "wall-tube" behaviour, but remain sufficiently small so that radial diffusion effects are not significant; the nozzle–electrode distance must be enough to prevent the back wall of the cell affecting the flow pattern over the electrode, but not so great as to allow the flow of the jet to be disturbed. Given these constraints, the limiting current is

$$I_L \propto R^{3/4} \nu^{-5/12} D^{2/3} a^{-1/2} V_f^{3/4} c_\infty$$

where R is the electrode radius, ν is the viscosity, D is the diffusion coefficient, a is the jet diameter, V_f is the volume flow rate, and c_∞ is the bulk concentration, and therefore specifying the errors as a function of I_L takes into account alternative values of these parameters. The error indicated by the value of I_L must then be adjusted if the electrode radius is not 1.637 mm, since, as discussed above, the main source of error is distortion of the current distribution near the centre of the electrode, and therefore the larger the electrode, the smaller will be the proportion of distorted current in the total, and the smaller the error. Thus the Tafel slope error should be multiplied by a factor of $(1.637/R)^{1.4}$, and the displacement of half-wave potential by a factor of $(1.637/R)^{1.25}$, these factors having been determined empirically from simulations for electrode radii in the range from 1.39 mm to 4.0 mm.

The error curves presented are scalable if the limiting current is adjusted in the same ratio as the solution conductivity, i.e. if the conductivity is halved, the same error will be obtained at half the limiting current shown. These curves, with the above adjustments for electrode radius if required, may therefore be used as a guide to the limiting currents and the conductivities which may be used within given limits of error. For instance, if an error limit of 0.002 V is required, then in the case of ferrocyanide oxidation at a typical flow rate of 0.08 $cm^3\ s^{-1}$, as recommended in Ref. [6], the limiting current indicated is 100 μA for 0.4M K_2SO_4, corresponding to a 1.5 mM concentration of electroactive species.

References

[1] M.B. Glauert, J. Fluid Mech., 1 (1956) 625.
[2] H. Gunasingham and B. Fleet, Electroanal. Chem., 16 (1988) 89.
[3] R.G. Compton, A.C. Fisher and G.P. Tyley, J. Appl. Electrochem., 21 (1991) 295.
[4] J.O. Dukovic, IBM J. Res. Dev., 34 (1990) 693.
[5] B.A. Coles, R.G. Compton and R.A. Spackman, Electroanalysis, 5 (1993) 41.
[6] C.M.A. Brett, A.M. Oliveira Brett, A.C. Fisher and R.G. Compton, J. Electroanal. Chem., 334 (1992) 57.
[7] W.J. Albery and C.M.A. Brett, J. Electroanal. Chem., 148 (1983) 201.
[8] R.C. Weast (ed.), Handbook of Chemistry and Physics, CRC Press, 55th edn., 1974.